
Enabling Persistent Autonomy for Underwater Gliders with Ocean Model Predictions and Terrain Based Navigation

Andrew Stuntz¹ Jonathan Kelly², and Ryan N. Smith^{1,*}

¹Robotic GNOME Laboratory, Fort Lewis College, Department of Physics & Engineering, Durango, CO, USA

²STARS Laboratory, Institute for Aerospace Studies, University of Toronto, Toronto, CANADA

Correspondence*:

Ryan N. Smith

Robotic GNOME Laboratory, Fort Lewis College, Physics and Engineering Department, Durango, CO, USA, rnsmith@fortlewis.edu

2 ABSTRACT

3 Effective study of ocean processes requires sampling over the duration of long (weeks to
4 months) oscillation patterns. Such sampling requires persistent, autonomous underwater vehicles,
5 that have a similarly long deployment duration. The spatiotemporal dynamics of the ocean
6 environment, coupled with limited communication capabilities, make navigation and localization
7 difficult, especially in coastal regions where the majority of interesting phenomena occur. In this
8 paper, we consider the combination of two methods for reducing navigation and localization
9 error; a predictive approach based on ocean model predictions and a prior information approach
10 derived from terrain-based navigation. The motivation for this work is not only for real-time state
11 estimation, but also for accurately reconstructing the actual path that the vehicle traversed to
12 contextualize the gathered data, with respect to the science question at hand. We present an
13 application for the practical use of priors and predictions for large-scale ocean sampling. This
14 combined approach builds upon previous works by the authors, and accurately localizes the
15 traversed path of an underwater glider over long-duration, ocean deployments. The proposed
16 method takes advantage of the reliable, short-term *predictions* of an ocean model, and the
17 utility of *priors* used in terrain-based navigation over areas of significant bathymetric relief to
18 bound uncertainty error in dead-reckoning navigation. This method improves upon our previously
19 published works by 1) demonstrating the utility of our terrain-based navigation method with
20 multiple field trials, and 2) presenting a hybrid algorithm that combines both approaches to
21 bound navigational error and uncertainty for long-term deployments of underwater vehicles. We
22 demonstrate the approach by examining data from actual field trials with autonomous underwater
23 gliders, and demonstrate an ability to estimate geographical location of an underwater glider to
24 < 100 m over paths of length > 2 km. Utilizing the combined algorithm, we are able to prescribe
25 an uncertainty bound for navigation, and instruct the glider to surface if that bound is exceeded
26 during a given mission.

27 **Keywords:** Terrain-based Navigation, Underwater Gliders, Persistent Autonomy, Localization, Underwater Navigation, Ocean Model

1 INTRODUCTION

28 Aquatic robots, such as Autonomous Underwater Vehicles (AUVs), and their supporting infrastructure
29 play a major role in the collection of oceanographic data (e.g., Godin et al. (2006), Paley et al. (2008) and
30 Whitcomb et al. (1999)). Actively actuated (propeller-driven) underwater vehicles have proven effective
31 in multiple sampling scenarios, however they have limited deployment endurance. The emergence of
32 buoyancy-driven vehicles, i.e., underwater gliders, has enabled greater energy savings and thus increased
33 endurance. With limited actuation, these vehicles are more susceptible to external forces, e.g., ocean
34 currents, resulting in poor navigational and localization accuracy underwater. This is exacerbated in coastal
35 regions, where current velocities can be the same order of magnitude as the vehicle velocity. Autonomous
36 underwater gliders provide an approach to observing ocean processes up close. These vehicles are capable
37 of long-term deployments, remaining out in the ocean for periods of time ranging from several weeks to
38 several months Davis et al. (2008). Although their horizontal speeds are only about 1 km/hr, their longevity,
39 coupled with the use of multiple gliders, can compensate by providing an extended temporal and spatial
40 series of observations.

41 Our work is motivated by the desire to enable intelligent data collection of complex dynamics and
42 processes that occur in a *coastal* ocean environments to further our understanding and prediction capabilities.
43 Of particular interest is the formation and evolution of Harmful Algal Blooms (HABs) in the Southern
44 California Bight (SCB); an oceanic region contained within 32° N to 34.5° N and -117° E to -121° E.
45 This region is under continued study to uncover the connections between small-scale biophysical processes
46 and large-scale events related to algal blooms, specifically blooms composed of toxin-producing species
47 (i.e., HABs) Jones et al. (2002); Schnetzer et al. (2007); Smith et al. (2010b). The long-term study utilizes
48 a team of two autonomous gliders (*He Ha Pe* and *Rusalka*), owned and operated by the USC Center for
49 Integrated Networked Aquatic PlatformS (CINAPS) team Smith et al. (2010b), to sample off the coast of
50 southern California. Field data examined within this paper were gathered during missions executed by these
51 vehicles. The Jet Propulsion Laboratory, California Institute of Technology, maintain a high-resolution,
52 large-scale regional ocean model for the SCB, and provided the model predictions used for our simulation
53 comparisons Vu (2008).

54 Autonomous gliders can spend in excess of 8 hours dead-reckoning under water, navigating by only
55 a compass, magnetometer and depth sensor. Frequent surfacing for position fixes limits the amount of
56 data that are collected during a deployment by decreasing the total time underwater, and by expending
57 excess energy for communication and localization while on the surface. Moreover, surfacing in potentially
58 hazardous locations (e.g., shipping lanes) puts the vehicle at risk. Maximizing time underwater significantly
59 reduces the ability of the vehicle to localize. Additionally, accurately reconstructing subsurface glider
60 trajectories can be difficult for long underwater transects; it is generally assumed that the traversed path of
61 a glider is the straight line connecting the the dive and surface locations, which is a poor assumption most
62 of the time.

63 To assist with energy savings, most gliders do not employ highly-accurate (high-energy) navigation
64 systems, but rely on dead-reckoning with a modest Inertial Measurement Unit (IMU). Regardless of
65 the specifications of the IMU, sensor drift is unbounded and navigational error increases with time.
66 During routine deployments in a coastal ocean environment in Los Angeles, CA, it was found that typical
67 underwater gliders experience roughly 650 m navigational error for each kilometer traveled Smith et al.
68 (2010c, 2012a). A combination of these factors can lead to poor experimental results. For example, Fig. 1
69 displays a planned path in black, and an actual execution of this planned path by a glider in white. This
70 poses difficulties in both plan execution in situ and reconstructing the actual traversed path of the vehicle

71 for analysis of scientific data. Additionally, for operations in cluttered environments, or near shipping lanes,
72 this error may put the vehicle at serious risk Pereira et al. (2013). With an Unscented Kalman Filter (UKF)
73 and inertial dead reckoning augmented with ocean model predictions, the authors have shown that this
74 error can be reduced to less than 500 m over a single kilometer of travel Smith et al. (2010c, 2012a); this is
75 still significant when trying to avoid a busy shipping lane or reconstructing a dataset. High-level planning
76 can provide assurance that the vehicle will follow a prescribed trajectory Pereira et al. (2013), however
77 we are always faced with potential navigation error during plan execution. In Smith et al. (2013), it is
78 shown that an approach solely based on ocean model predictions breaks down in regions of significant
79 bathymetric relief; where ocean models have poor prediction capabilities. However, these regions of
80 significant bathymetric relief are exactly where a terrain-based navigation approach is able to perform well.
81 Here, we examine the utility of integrating terrain-based navigation methods into an existing framework for
82 improving the navigational accuracy of underwater gliders. Specifically, we propose to utilize ocean model
83 predictions within a UKF to improve planning and navigation capabilities, while additionally incorporating
84 a terrain-based navigation method for localization during plan execution.

85 Areas of significant productivity in the coastal ocean are highly correlated to locations of significant
86 bathymetric relief, e.g., algal blooms Sekula-Wood et al. (2009); Fulton-Bennett (2005); Horner et al.
87 (1997); Anderson et al. (2002); Kudela et al. (2005) and ocean fronts Mancho et al. (2008); Ferrari (2011);
88 Zhang et al. (2013). In these areas, every path traversed by an AUV has a depth signature that is highly
89 variable, and becomes increasingly unique the longer the trajectory becomes. These specific deployment
90 locations and science motivations enhance the utility of terrain-based methods to increase navigation
91 accuracy and localization for long-duration missions.

92 The use of prior information in the form of predictive ocean models has been shown to improve mission
93 accuracy and execution during field trials Smith et al. (2010c, 2012a). While these models have become
94 quite advanced, they are still generally discrete and deterministic in nature. Specifically, there is no metric
95 provided on the confidence or covariance of the predicted variable, and accurate interpolations of the
96 discrete measurements requires sophisticated data processing algorithms to augment the predictions. The
97 developers of both ROMS and HOPS have investigated producing ensemble forecasts for their model. This
98 method perturbs initial and/or boundary conditions to produce a set of forecasts. This ensemble forecast
99 provides a distribution of potential outcomes, however the sample size is often too small (~ 12) to provide
100 a meaningful variance measure of the prediction. These ensembles can provide an accuracy estimation of
101 the model output, however this is more related to the sensitivity of the numerical model to the inputs rather
102 than the actual physical variability of the ocean inherent within the domain of the model. The size of the
103 ensemble forecast is limited only by computational power and time. However, as models provide the most
104 accurate predictions in the times closest to observations and measurements, we cannot spend an excessive
105 amount of time computing all the possible ensemble outcomes. So, we are faced with the compromise of
106 working to produce the most accurate models utilizing a minimal set of resources, or utilizing additional
107 resources to augment the computation of model reliability and variability. In current research, several
108 assimilation techniques, e.g., Kalman filter-based ensemble forecasts Rixen et al. (2009), and variational
109 schemes, e.g., 4DVar Powell et al. (2008), are under investigation in the modeling community, with the
110 goal to get the model output closer to the observed values.

111 Predictive models have been exploited in previous AUV mission planning efforts, where a main focus
112 has been to compute energy-optimal paths, as the majority of applications utilize propeller-driven, short-
113 duration (< 24 hr) AUVs. The work in Garau et al. (2005) makes use of the A* search procedure to harness
114 the inherent spatial variability of currents and minimize expended energy. Similarly, the authors in Alvarez

115 et al. (2004) employ a genetic algorithm to generate energy-conserving trajectories for an AUV subject
116 to time-varying currents. Research in Witt and Dunbabin (2008) explores the utility of predictive models
117 to aid in avoiding land masses exposed by ebbing tides, while the investigation in Kruger et al. (2007)
118 examines how predictions can be used to ‘ride’ currents in estuarine and riverine environments. Although
119 the methodologies, domains and applications are different, the underlying models used are all deterministic,
120 providing a fixed value for the current at a specified location and time. Much recent research in robotics
121 leverages probabilistic planning and control methods, and has the potential to be applied to the marine
122 domain, e.g., Ono and Williams (2008); Rao and Williams (2009); Hollinger et al. (2012). Hence, it is
123 critical to understand the probabilistic nature and/or variability of the priors that will best enable ocean
124 sampling, e.g., predictive ocean models.

125 However, even with good ocean models, underwater gliders still use dead-reckoning while underway. As a
126 proprioceptive device, an IMU is one navigation aid that can be utilized in underwater environments without
127 requiring external electromagnetic signal reception. IMU error sources and their effects on navigation
128 performance are discussed in Flenniken et al. (2005), which demonstrates that even using tactical-grade
129 sensors, the inevitable drift is still too high to mitigate substantial trajectory errors. Navigation is not
130 reliable using IMU data alone, especially when localization fixes are scarce and sensor drift cannot be
131 bounded.

132 A detailed survey of recent advances and current challenges in underwater navigation, summarizing
133 existing work on Terrain Based Navigation (TBN) for underwater vehicles, is provided in Kinsey et al.
134 (2006). One clearly identified shortcoming of TBN in the aquatic environment is the lack of accurate,
135 high-resolution maps of the sea floor in many regions. Additionally, sensor limitations, especially the
136 limitations of optical range sensors, substantially restrict TBN underwater. In Kinsey et al. (2006), it is
137 concluded that improved navigation will enable new missions that would previously have been considered
138 infeasible or impractical. The idea of terrain based navigation is not new; significant research was carried
139 out on the use of TBN for long-range missile guidance prior to the development of the GPS satellite
140 network Golden (1980). Here, we apply a similar concept to an underwater glider.

141 Recent work by Lagadec on TBN under ice Lagadec (2010) has demonstrated the feasibility of using
142 a particle filter for long term glider navigation. Lower relief maps, with a resolution of 2 km, of regions
143 above the arctic circle were sufficient to navigate with reasonable accuracy (~ 1 km accuracy, with a
144 mean accuracy of approximately 8 km in one simulation). The study suggests that for real deployments,
145 technological advances would be necessary to achieve the required navigation performance. However,
146 higher relief bathymetric maps could facilitate the implementation of a TBN that operates online, in real
147 time. The primary limitation of the technique presented in Lagadec (2010) was the lack of an accurate
148 terrain map, which does not invalidate the methodology used. A significant difference between this method
149 and the proposed is that the use of a particle filter relies both on an accurate terrain map *and* a dynamic
150 model to propagate the state. Our proposed TBN method does not rely on an underlying dynamic model.
151 Although, adding a dynamic vehicle model to our TBN approach will improve the presented results.

152 A number of other studies have utilized particle filters as part of a TBN framework for underwater vehicles
153 Anonsen and Hallingstad (2007, 2006); Gustafsson et al. (2002); Lagadec (2010). The particle filter is
154 suitable as a solution to the TBN problem because it is probabilistic (and therefore captures environmental
155 uncertainty), and because it naturally incorporates the property that the longer a path is traversed, the
156 more likely a single solution will emerge. Again, filtering requires a known motion model for the vehicle,
157 in order to weight possible trajectories according to the dynamics achievable by the system. A simple
158 motion model has limitations when applied to underwater gliders, however, as a significant portion of

159 the glider motion is driven by ocean currents that can be of the same order of magnitude as the nominal
160 vehicle velocity. Hence, the accuracy of a glider motion model depends heavily on an ability to predict
161 ocean currents, which can be difficult in highly dynamic environments like the coastal ocean. The method
162 proposed herein is developed as a model-free approach to the TBN problem, using only the acquired water
163 depth data and the initial heading to the next prescribed waypoint. Although this approach is deterministic
164 in nature, it does not rely on a vehicle or ocean model.

165 This paper examines the combination of two methods for improving both navigation and localization, not
166 only for real-time state estimation, but also for accurately reconstructing the actual path that the vehicle
167 traversed to contextualize the gathered data. The overarching goal is to provide an online method for
168 autonomous gliders to accurately navigate in coastal regions. We combine a predictive approach that
169 incorporates glider motion derived from an IMU and ocean model predictions into an UKF with a real-time,
170 terrain-based navigation (TBN) algorithm. The UKF algorithm provides mission planning and a navigation
171 strategy, while the TBN algorithm provides accurate localization during mission execution. The UKF
172 integrates data from an IMU, and the TBN algorithm utilizes only the depth, altitude and initial compass
173 heading from start to goal, thus the entire system operates *model-free*. Practically, TBN for underwater
174 vehicles is limited by the altitude sensor's ability to *see the ground*, which is not a limiting factor for most
175 coastal and shallow (< 200 m) operations.

176 The presented approach builds upon prior work by the authors in both the incorporation of ocean models
177 for planning and the use of terrain-based navigation for real-time localization and path reconstruction
178 Stuntz et al. (2015). The primary contributions of this paper combine these approaches into a single,
179 implementable algorithm, as well as extends existing results in the following four ways.

- 180 1. We apply our TBN algorithm to multiple glider missions with varying trajectory length, mission time
181 and bathymetric relief, further demonstrating the utility of the proposed method.
- 182 2. The additional results from extended applications of the TBN algorithm demonstrate the capability of
183 the proposed method to accurately reconstruct the actual paths that gliders followed during mission
184 execution.
- 185 3. We present an algorithm that combines the predictive ocean model-based UKF method with the
186 TBN algorithm to provide a robust methodology for maintaining a fixed navigational uncertainty for
187 underwater gliders.
- 188 4. We demonstrate that the combination of our two methods into a single algorithm can a) be run in real
189 time, on-board an underwater glider, and b) maintains a prescribed navigational error for all executed
190 missions.

191 The proposed methodologies have been tested with data from multiple deployments of Slocum
192 autonomous gliders off the coast of California, USA. Results are presented that demonstrate a significant
193 increase in navigational accuracy compared with previously reported results.

2 BACKGROUND

194 2.1 Autonomous Underwater Gliders

195 The vehicle for this study is a Webb Slocum autonomous underwater glider Webb Research Corporation
196 (2008) as seen in Fig. 2. A Slocum glider is a 1.5 m (length) by 21.3 cm (diameter), torpedo-shaped vehicle
197 designed for long-term (~ 1 month) ocean sampling and monitoring Schofield et al. (2007), Griffiths

198 et al. (2007). These vehicles *fly* through the water driven entirely by a variable buoyancy system. Wings
199 convert the buoyancy-dependent vertical motion into forward velocity. Inflection points occur at depths
200 and altitudes set in the user-defined mission plan. Thus, the glider navigates by dead-reckoning between
201 waypoints with a sequence of dives and climbs (yo-yos), forming a vertical sawtooth pattern.

202 Gliders are utilized for their deployment endurance, as they provide an optimal method for generating
203 high-resolution spatial and temporal data with minimal energy expense. Sophisticated and power-hungry
204 navigational instruments are not common due to the reduction in deployment duration resulting from
205 their increased power consumption. For similar reasons, on-board decision making and computation are
206 generally not performed. A Slocum glider includes a GPS receiver for localization at each surfacing. In
207 addition to the GPS receiver, a typical glider carries a PNI TCM2 attitude sensor and a SBE 41CP pressure
208 sensor on-board. The TCM2 incorporates an electronic compass, a three-axis magnetometer and a two-axis
209 tilt sensor, and is able to provide attitude data at a user-selectable rate of 1 to 30 Hz; heading accuracy
210 is $\pm 1^\circ$ RMS, and roll/pitch accuracy is approximately $\pm 0.2^\circ$ RMS. The SBE measures pressure with an
211 RMS accuracy of 2 decibars, or depth with an RMS accuracy of 2.03 m near the water surface, at a rate of
212 1 Hz. In addition, each glider incorporates a Sea Bird non-pumped, low drag conductivity, temperature,
213 and depth package. A 500-PSI pressure transducer is used for the depth measurement. An Airmar altimeter,
214 0 – 100 m range transducer and electronics are supported on the Displacement Piston Pump Cylinder. The
215 transducer is mounted such that it is parallel to a flat sea bottom at a dive angle of nominally 26 degrees.

216 2.2 Dead Reckoning Error Estimation

217 Based on the results of initial tests presented in Smith et al. (2010b), we are motivated to further
218 investigate the improvement of navigational capabilities of gliders by use of TBN. Since a glider depends
219 solely upon dead reckoning for subsurface navigation, the uncertainty in the estimated state will grow
220 without bound. For our applications in the coastal regions of Southern California, we generally require
221 the vehicle to surface frequently (every 3 – 6 hours), see e.g., Smith et al. (2010b,a, 2011a). Since we
222 acquire GPS ground truth relatively frequently, we are able to bound the growth of the state estimation
223 error. This provides a baseline expected error for the assessment of navigational accuracy and precision. In
224 this paper, we are interested in better localization while underwater between waypoints to enable more
225 accurate reconstructions of executed trajectories.

226 During a deployment, a Slocum glider navigates by the following method: when navigating to a new
227 waypoint, the present location L of the vehicle is compared to the next prescribed waypoint in the mission
228 file (W_i), and a bearing and range are computed for execution of the next segment of the mission. The
229 geographical location at the extent of the computed bearing and range from L is the aiming point A_i . The
230 vehicle dead-reckons with the computed bearing and range towards A_i , with the intent of surfacing at W_i .
231 The computed bearing is not altered, and the glider must surface to make any corrections or modifications
232 to its dive plan. When the glider determines that it has traveled the requested range at the specified bearing
233 (based on speed over ground estimation from the previous dive), it surfaces and acquires a GPS fix. If
234 the vehicle surfaces within a given range of W_i , the waypoint is determined to be *achieved*. Positional
235 error between the actual surfacing location and W_i is computed, and is fully attributed to environmental
236 disturbances, i.e., ocean currents. A depth-averaged current vector is computed, and this is factored in
237 when computing the range and bearing to W_{i+1} . Hence, A_i is in general not in the same physical location
238 as W_i , and rarely does the glider ever surface at W_i . It is of interest to note that A_i is computed from the
239 error observed in the previously executed leg, and does not make a prediction or take into account the fact
240 that the vehicle may not be moving through a similar current regime.

241 2.3 Terrain-Based Navigation

242 Prior to satellite-based navigation, e.g., GPS, long-distance navigation systems were developed for
 243 missiles Golden (1980). Data from an embedded altimeter were compared to ground elevations that were
 244 provided in a stored map or look-up table. The navigational accuracy of this method is dependent upon the
 245 resolution of the underlying topography map and the accuracy of the elevation measurement; both very
 246 good for terrestrial applications. This system became redundant after the introduction of GPS, although it
 247 is still a useful navigational aid for GPS-denied environments, e.g., underwater. Until recently, the utility of
 248 terrain-based navigation for underwater vehicles was low due to the poor resolution of bathymetric maps.
 249 Updated bathymetry maps with higher resolution provide motivation for revisiting the application of this
 250 method for low-power, accurate navigation underwater. Additionally, given the increase in accuracy of
 251 low-cost sensors for dead-reckoning, e.g., IMUs, and increased skill of ocean models, it is of interest to
 252 investigate a combined approach to increasing underwater navigation.

3 UNSCENTED KALMAN FILTER AND OCEAN MODEL PREDICTION ALGORITHM

253 Through previous research efforts, we have developed a simulation tool for glider missions in the SCB
 254 that incorporates the ROMS predictions of the 3D velocity field Smith et al. (2010c, 2012a). We fuse
 255 the measurements from the sensors (either actual in real-time or simulated post priori) into an Unscented
 256 Kalman Filter (UKF) to estimate the position, attitude and velocity of the vehicle over time Julier and
 257 Uhlmann (2004).

258 The UKF is a Bayesian filtering algorithm which employs a statistical local linearization procedure to
 259 propagate and update the system state. For nonlinear systems, this approach typically produces significantly
 260 more accurate estimates than the analytic local linearization employed by the well-known Extended Kalman
 261 filter (EKF) Huster and Rock (2003). In our case, the 10×1 state vector is

$$\mathbf{x}(t) = \left[(\mathbf{p}^W(t))^T \quad (\bar{q}_B^W(t))^T \quad (\mathbf{v}^B(t))^T \right]^T, \quad (1)$$

262 where $\mathbf{p}^W(t)$ is the position of the glider in the world (UTM) frame, $\bar{q}_B^W(t)$ is the unit quaternion that
 263 defines the attitude of the glider body relative to the world frame, and $\mathbf{v}^B(t)$ is the velocity of the glider in
 264 the body frame. This simple kinematic model is sufficient for this application of long-range planning. A
 265 primary motivation for our choice of the UKF is its performance with a more sophisticated (and nonlinear)
 266 dynamic model of the glider, which we are exploring in a parallel effort.

For our simulation, we assume that the glider follows a nominal, linear sawtooth trajectory, and that the vehicle angular rotation rate and linear acceleration are driven by white, zero-mean Gaussian noise processes represented by the vectors $\eta_q(t)$ and $\eta_v(t)$, with covariance matrices \mathbf{Q}_q and \mathbf{Q}_v , respectively. The system state evolves in continuous time according to

$$\dot{\mathbf{p}}^W(t) = \mathbf{C}(\bar{q}_B^W(t)) \mathbf{v}^B(t), \quad (2)$$

$$\dot{\bar{q}}_B^W(t) = \frac{1}{2} \Omega(\eta_q(t)) \bar{q}_B^W(t), \quad (3)$$

$$\dot{\mathbf{v}}^B(t) = \eta_v(t), \quad (4)$$

267 where $\mathbf{C}(\bar{q}_B^W(t))$ is the direction cosine matrix corresponding to the unit quaternion $\bar{q}_B^W(t)$, and $\Omega(\eta_q(t))$
 268 is the quaternion kinematic matrix, relating the rate of change of the orientation quaternion to the body
 269 frame angular velocity Stevens and Lewis (2003).

270 The effects of the currents on the glider are incorporated as a concatenation of the contributions from
 271 the velocity of the glider in the water column, and the velocity of the water column itself (i.e., the ocean
 272 currents). The modified process model for the glider position is then

$$\dot{\mathbf{p}}^W(t) = \mathbf{C}(\bar{q}_B^W(t)) \mathbf{v}^B(t) + \mathbf{v}_{\text{ROMS}}(t), \quad (5)$$

273 where $\mathbf{v}_{\text{ROMS}}(t)$ is the predicted water current velocity, found by spatiotemporally interpolating the ROMS
 274 (or other ocean model) prediction.

275 Our improved navigation strategy involves attempting to predict, based on the our kinematic model and
 276 the ROMS data, how far the glider will drift away from the desired trajectory. We aim to limit the drift such
 277 that the distance between the glider's position and the planned trajectory is never larger than the primary
 278 axis of the UKF 3σ uncertainty ellipse. Equivalently, at least one point on the trajectory should lie within
 279 the 3σ uncertainty ellipse. For the simulations here, 3σ corresponds to ~ 600 m.

280 The initial steps follow those for a normal mission as discussed in Section 2.2. We run a prediction step
 281 using a deterministic, discrete kinematic model incorporating ROMS prediction data, for a given surfacing
 282 time. The glider begins on the surface, and computes a heading and bearing location A_i to reach W_i based
 283 on the depth-averaged currents experienced during the previous leg. The glider dives, and surfaces upon
 284 reaching W_i or after a duration T hours has elapsed.

285 To begin the simulated mission, we compute an initial depth-averaged current by running for T hours
 286 and finding the offset from the prescribed path as a one-time initialization. This initial drift offset is then
 287 used to adjust the glider heading (in the opposite direction) as the difference in angle between our expected
 288 and (simulated) trajectory.

289 Next, we simulate the full dive profile, using ROMS current predictions and the kinematic model above,
 290 using the UKF. This provides an expected surfacing location with an associated uncertainty ellipse. If,
 291 at the end of T hours, the glider surfaces more than 3σ away from the desired trajectory, the mission
 292 terminates. Otherwise, the simulation continues with another dive as outlined in Section 2.2.

293 We iteratively simulate the execution of a segment 25 times; $T_j = \{2, 2.25, 2.5, \dots, 7.75, 8\}$ hours. For
 294 each j , a path segment with $T = T_j$, represented by $\gamma_i(T_j)$, is considered successful when the final surfacing
 295 on a segment is within $\delta = 1000$ m of the goal waypoint, and at all surfacings along the segment the distance
 296 from the glider to the prescribed path remains less the 3σ uncertainty ellipse, i.e., the glider remained
 297 within 600 m of the prescribed path. For each γ_i , we compute $\mathcal{S} = \{\cup_j \gamma_i(T_j) | \gamma_i(T_j) \text{ is successful}\}$, the
 298 set of all successful executions. Then, for the entire path, we compute the desired surfacing interval S to be

$$S = \min_i \max_j \{T_j | \gamma_i(T_j) \text{ is successful}\} \quad (6)$$

299 Thus, for a prescribed mission, the UKF Algorithm outputs a proposed surfacing interval S , which may
 300 define intermediate waypoints between the initially prescribed path waypoints. For each of the computed
 301 waypoints, the UKF Algorithm provides 1) a predicted surfacing location which is given by the computed
 302 3σ uncertainty ellipse, and 2) an aiming point A_i based on the ocean model predictions to aid in improving

303 navigation to the next waypoint. Further details and implementations of this approach are presented in
 304 Smith et al. (2010c, 2012a, 2013).

4 TERRAIN-BASED NAVIGATION ALGORITHM

305 To address the issues of poor ocean model predictions along the shelf break region, and to provide a method
 306 for localization while underwater, we present a least-squares optimization method for determining the
 307 path traversed by the glider based on gathered depth data; a terrain-based navigation approach. We utilize
 308 publicly available maps provided by the Southern California Coastal Ocean Observing System (SCCOOS),
 309 which provide 30 arc second grid resolution SCCOOS (2009). The data is accurate to grids of 0.0008° of
 310 latitude and longitude.

311 The Least Squares Error-Terrain Based Navigation (LSE/TBN) algorithm is presented in detail in Stuntz
 312 et al. (2015) and reproduced here in Algorithm 1. The LSE/TBN Algorithm takes as input the start location,
 313 heading to proposed ending location or aiming point A_i , and gathered vehicle depth and altitude data. The
 314 output is predicted latitude and longitude at each time epoch the algorithm is executed.

Algorithm 1: LSE/TBN Algorithm

```

TotalDistance ← Distance between Start Latitude and Longitude and Ending Latitude and Longitude
while  $i \leq \text{TotalDistance}$  do
  Discretize bathymetry data
   $xc \leftarrow$  find closest grid value to Starting Longitude
   $yc \leftarrow$  find closest grid value to Starting Latitude
  DP ← distance to closest edge of grid
  for  $n \leq -90 + \text{Starting Direction} + 90$  do
     $T(n) \leftarrow$  Generate Paths around starting location
    D1 ← Distance traveled in step
    Points ← Depth data based on length of D1
     $T_w(n) \leftarrow$  Weight the paths based on trajectory
  end for
  while  $n \leq \text{length}(P_o)$  do
     $R^2 \leftarrow (T(n) - \text{Points})^2$ 
     $P_o(n) = T_{wi}(n) \times W_T + R^2(n) \times W_R$ 
    P ← min( $P_o$ , 0)
    n ← n+1
  end while
  Start Latitude ← Latitude at end of P
  Start Longitude ← Longitude at end of P
   $i \leftarrow i + D1$ 
end while

```

315 Acquired depth data are smoothed over time to handle sensor noise and hysteresis. Some of the error
 316 is a result of the fixed angle of the altimeter, causing altitude measurements to be inaccurate during
 317 the ascent portion of the yo-yo trajectory path that gliders execute. These data were smoothed using a
 318 standard deviation rejection algorithm Taylor (1996). During real-time implementation, we break the
 319 deployment into pieces consisting of only the segments when the vehicle is diving. These segments are
 320 then concatenated to reconstruct the actual path. This implementation method allows for computation to
 321 occur during each ascent along the path.

Within Algorithm 1, path options are generated by sweeping the area around the starting location to generate 180 different path options, generating one path option for every compass degree from -90° of the expected direction to $+90^\circ$ of the expected direction. Equations 7a-9b describe how this is done. First, the point (x, y) is translated to the origin (x_o, y_o) .

$$x_o = |x - startlong| \quad (7a)$$

$$y_o = |y - startlat| \quad (7b)$$

Then, using a rotation formula the points are rotated about (x', y') .

$$xa = \cos(\theta) \times x_o + \sin(\theta) \times y_o \quad (8a)$$

$$ya = -\sin(\theta) \times x_o + \cos(\theta) \times y_o; \quad (8b)$$

Each point is then sent back (translated back) to its original location by adding it to the original point (x, y) .

$$x' = xa + startlong \quad (9a)$$

$$y' = ya + startlat \quad (9b)$$

322 The length of each possible segment is chosen by picking the closest point of the bathymetric grid to the
 323 *startlat* and *startlong*. This keeps the step size lengths between $.0001^\circ$ and 0.0008° , which is less than or
 324 equal to the resolution of the SCCOOS bathymetric maps for each step. The expected direction to initialize
 325 the iterative algorithm is taken to be the azimuth from the projected trajectory. An example of the generated
 326 path options can be seen in Fig. 9. Each path segment length is computed using the Haversine formula.
 327 Using this length, we determine the number of data points (DP) within the segment.

328 A linear least-squares approximation is used to compute the error for each path segment between the
 329 measured water depth values and an interpolated bathymetric map. The linear least-squares method solves
 330 an over determined system by minimizing the error of the data points to a given line, $f(x) = m \times x + b$, as
 331 shown in Eq 10.

$$R^2 = \sum_{i=1}^n [y_i - f(x_1, x_2, x_3 \dots x_n)]^2 \quad (10)$$

332 The R^2 values are normalized between 0 and 1 to provide a weighting for each path segment.

333 Given the prescribed trajectory we additionally assign a weight (T_w) to each path segment, based on how
 334 close the azimuth is to the initially prescribed trajectory. Assume the prescribed trajectory has an azimuth
 335 of 92° from starting point to goal location. The computed path segments then have an azimuth range from
 336 1° to -1° . We assign the preferred direction a value of $T_w = 90^2$, and decrease as the segments diverge
 337 away from this direction. Thus, an azimuth of 92 would have a weight of $T_w = 90^2$, an azimuth of 91 or 93
 338 would have a weighting of $T_w = 89^2$, an azimuth of 2 would have a weighting of $T_w = 1^2$, etc. The path
 339 segments at each epoch are then weighted using the weighting function T_{w_i} shown in Eq. 11.

$$T_{w_i} = 1 - [(T_{w_i} - \min(T_w)) / (\max(T_w) - \min(T_w))] \quad (11)$$

340 Since T_{w_i} is maximized about the trajectory it is normalized between 0 and 1, then subtracted from one to
 341 get a minimization criterion.

342 Finally, a path segment is chosen based on the cost function shown in Eq. 12. The parameter α is initially
343 set to 0.5, and seeds the algorithm. Altering α allows for emphasizing a preferred heading, e.g., close to
344 the compass heading between the start location and goal location, in regions of minimal bathymetric relief;
345 regions where multiple path segments have identical R^2 values from the least-squares optimization. As the
346 bathymetric relief approaches zero over the path, $\alpha \rightarrow 1$ since the R^2 values for all paths will approach
347 equality and will not contribute meaningful information to the optimization criterion.

$$P_o = T_{w_i} \times \alpha + R^2 \times (1 - \alpha) \quad (12)$$

348 Since both T_{w_i} and R^2 are normalized between zero and one the weighting factors also stay between zero
349 and one so that neither T_{w_i} or R^2 dominate.

350 The algorithm then initializes the end of the chosen path segment as the new start point and the process
351 repeats itself until it has utilized all of the available depth data. Further details are presented in Stuntz et al.
352 (2015).

5 FIELD EXPERIMENTS

353 Hundreds of glider missions have been successfully completed off the California coast over the last few
354 years by the University of Southern California CINAPS team Smith et al. (2010b). For this paper, we utilize
355 data gathered from multiple deployments of Slocum gliders in both Monterey Bay and off the coast of Los
356 Angeles, CA USA. These data are used to validate the proposed methods to better reconstruct executed
357 trajectories for science analysis and provide better real-time localization while underwater. Commonly,
358 glider trajectories are represented as straight lines underwater by connecting adjacent surfacing locations.
359 The fact is that glider motion is hardly a straight line, as they are continually moved underwater by ocean
360 currents and continual correction with poor navigation systems. The proposed method will provide better
361 mission planning, navigation and trajectory reconstruction, thus enabling a clearer understanding and
362 contextualization of the data that these vehicles collect.

363 The experiments in this study were conducted in southern California between 14 July and 3 August, 2011,
364 and in Monterey Bay during October 2010. During these times, multiple gliders were deployed, executing
365 pre-defined sampling missions, yo-yoing between 2 and 100 m. Further details of these standard missions
366 can be found in Smith et al. (2011a,b). From all of the surfacing locations during the mission executions,
367 we selected those where the subsequent surfacing *hit a waypoint*. Thus, we selected the dives for which
368 we knew the start location at the surface L , the desired waypoint W_i , the aiming point A_i , and the actual
369 surfacing location S of the vehicle for each segment examined. For southern California, these selected
370 mission segments comprise 34 surfacing events over a span of 21 days. For Monterey Bay, we present one
371 mission demonstrating of the proposed TBN algorithm.

6 UNSCENTED KALMAN FILTER AND OCEAN MODEL PREDICTION RESULTS

372 For each of the 34 missions considered in the SCB, Fig. 3 displays the surfacing error (distance between the
373 desired waypoint and the actual surfacing location) versus the length of the trajectory. Note the linear trend
374 of the data; the longer that the glider dead-reckons underwater, the greater the surfacing error. Given that
375 the surfacing error is directly correlated to the distance that the vehicle traveled underwater, we normalize

376 this by use of Eq.(13) for an equivalent comparison across all 34 missions.

$$\text{Error}_{\text{Normalized}} = \frac{d_g(S, W_i)}{d_g(L, W_i)} \quad (13)$$

377 Here $d_g(x, y)$ is the geographical distance between x and y . Figure 4 displays a heat-map surface plot of
 378 this normalized surfacing error within the SCVB for each of the 34 actual surfacing instances. Regions in
 379 blue indicate small error, while red regions are indicative of large error. The stars represent the waypoints
 380 that the two gliders were trying to achieve. The heat map is computed using a cubic interpolation of the 34
 381 data points.

382 Comparing these errors with water depth, as shown in Smith et al. (2013), we note that the largest
 383 errors occur near shore and in the shelf break portion of the region. These large errors are attributed to the
 384 following.

- 385 1. Regional forcing drives upwelling across the shelf and creates strong and complex currents in the shelf
 386 region, which cannot be modeled well.
- 387 2. Two of the northernmost waypoints are less than one kilometer apart, and are used as a holding pattern
 388 between missions. Since the glider must travel by executing an integer number of yos, overshooting
 389 the waypoint is likely due to the short baseline distance; the normalized error for geographically close
 390 waypoints.

391 We implemented our developed UKF model to execute all 34 missions using the ocean current predictions
 392 from ROMS for the respective day and time of actual execution. Figure 5 displays the surfacing error versus
 393 the length of the trajectory for these simulations. The linear trend is not as evident in Fig. 5 as previously
 394 seen in Fig. 3, with much more dispersion in the shorter-length missions. Figure 6 displays a heat-map
 395 surface plot of this normalized surfacing error within the deployment region for each of the 34 simulated
 396 surfacing instances. Regions in blue indicate small error, while red regions are indicative of large error. A
 397 normalized error of value > 1 indicates a surfacing error greater than the length of the prescribed trajectory.
 398 The stars represent the waypoints that the two gliders were trying to achieve. The heat map is computed
 399 using a cubic interpolation of the 34 data points.

400 Here, the largest errors are seen directly along the shelf break; a region where the bathymetry changes
 401 rapidly as you move towards shore. Note that the scale is different from Fig. 4, with the error along the
 402 shelf break > 1 ; the surfacing error was larger than the actual length of the prescribed trajectory. It is
 403 understandable that a model would have trouble predicting currents in this complex region.

404 A detailed comparison of these results is presented in Smith et al. (2013), and shows a good match
 405 between model predictions and the results of field trial validation for a small region within the SCB. This
 406 demonstrates the utility of ocean model predictions within our proposed UKF framework for mission
 407 planning and navigation in a coastal region. We note that with just this method, error still exists in the
 408 surfacing location. Hence, there is a need for a localization method to determine the actual path that the
 409 glider followed.

410 6.1 Terrain-Based Navigation Results

411 6.1.1 Monterey Bay Deployment

412 We demonstrate the effectiveness in localization and path reconstruction of our TBN algorithm on a
 413 glider deployment in Monterey Bay, CA USA executed during the Monterey Bay Aquarium Research

414 Institute CANON experiments in October 2010 Chavez (2010). The deployment region is focused on the
415 northern shelf in Monterey Bay, referred to as the algal bloom incubator. The terrain in this region is varied
416 and the bathymetry maps are high-resolution. The Glider He Ha Pe Smith et al. (2010b) was deployed
417 in Monterey Bay in October of 2010. Its start position was (36.8431, -121.9204) and it was headed for
418 (36.8097, -121.9041). The actual final surfacing location was (36.8415, -121.8694); a ~ 4.7 km error
419 in surfacing location. The vehicle traveled a straight line distance of approximately 4.5377 km from its
420 initial position to its ending position. The deployment can be seen in Fig. 7. Given the drastic difference
421 in prescribed surfacing location and actual surfacing location, this mission is an excellent candidate for
422 demonstrating our method. The Glider He Ha Pe started at the yellow pin in Fig. 7. The glider surfaced at
423 the green pin, but was attempting to head towards the red pin in Fig. 7. Note that the glider surfaced at the
424 location that it *thought* was the prescribed waypoint. Thus, we see a navigational error in the onboard INS
425 of approximately 4,688 m. The glider actually traversed an area with a depth relief of less than 0.4% with
426 raw, recorded depth data showing a relief of approximately 1.7%.

427 Applying the LSE/TBN Algorithm to the chosen trajectory in Monterey Bay, CA, we see a difference
428 between the predicted surfacing location and the actual surfacing location of 55 m. This is the total
429 navigation error over the entire 4.54 km trajectory. The algorithm utilized a weighting factor (α) of 0.5.
430 Figure 10 shows the path computed by the LSE/TBN Algorithm. For this path, the LSE/TBN Algorithm
431 iterated 69 times. A top-down view of the computed trajectory is presented in Fig. 11.

432 The predicted path is laid over the bathymetry map and presented in Fig. 10. Here, we show the actual
433 ending point, predicted ending point, and initial goal. The path followed rises approximately 20 m over a
434 length of 4565.7 m. This is an overall depth relief of approximately less than 0.5%. The distance actually
435 traveled was 4537 m, a difference of 29 m (0.6% error) from the predicted distance traveled. The distance
436 between the actual surfacing location and the predicted surfacing location was 55 m. Some of this error
437 may be attributed to the drift a glider experiences as it sits on the surface waiting for a GPS fix. Further
438 details and analysis are presented in (Stuntz et al., 2015).

439 6.1.2 Southern California Bight Results

440 Further validation of the proposed TBN algorithm was demonstrated by examining multiple missions
441 from the Southern California Bight glider missions that were presented in Section 3. We examined 8 of the
442 34 missions, which occurred in those regions where the ocean model prediction algorithm demonstrated
443 poor results; shallow water and across the shelf break where there is significant bathymetric relief. The
444 locations of the selected missions overlaid on a bathymetric heat map is presented in Fig. 13. Here, red
445 is shallow and blue is deep, the white stars identify the starting location for each mission examined. The
446 results of the TBN algorithm applied to these missions is presented in Table 1. Here, the first column
447 presents the overall length of the path given by our TBN algorithm. The second column provides the
448 prescribed path length as the straight-line distance between start and goal waypoints. The third column
449 gives the distance between the actual surfacing location and the predicted surfacing location given by our
450 TBN algorithm. The fourth column presents the distance between the predicted surfacing location from our
451 TBN algorithm and the actual goal waypoint. The final column displays the distance between the actual goal
452 waypoint and the actual surfacing location of the glider during field trials. Note that during the field trials,
453 the glider was not executing any of the algorithms proposed in this manuscript, hence it was only relying
454 on dead-reckoning navigation and the actual surfacing location was not biased or affected by the proposed
455 methods. Figure 12 displays the surfacing error versus the length of the trajectory for these simulations. We
456 note that there is no noticeable trend to these data, with predicted surfacing errors seemingly not dependent
457 upon distance traveled as was the case shown in Fig 3. Most noticeably is a similar error in navigation for

458 paths of 600 m and 2500 m. This similarity is a result of the TBN algorithm depending primarily upon
459 the resolution of the underlying bathymetry map, which is 0.0008° or approximately 88 m at the latitude
460 of southern California where the missions were executed. The results from the SCB compare well with
461 those presented for the Monterey Bay data set. This demonstrates the ability of our proposed TBN method
462 to augment the UKF Algorithm for a hybrid algorithm for mission planning and localization to enable
463 persistent operations.

7 COMBINING PRIORS AND PREDICTIONS

464 We have presented two methods for aiding underwater gliders to increase navigational accuracy, as well as
465 reconstruct the traversed path after execution. The ocean model prediction method utilizes *predictions* to
466 aid in plan execution in the uncertain ocean environment. The terrain-based algorithm utilizes *priors* in the
467 form of bathymetry maps to accurately plot the traversed path of the vehicle while underway. Each method
468 has shown to increase overall accuracy for navigation and the ability of gliders to reach the designated
469 waypoint. However, each method demonstrates poor results over a subset of the experimental domain
470 that are complimentary to one another. Ocean model predictions are not able to predict the currents well
471 over areas of large bathymetric relief, and the accuracy of the model degrades over time. Terrain-based
472 navigation demonstrates excellent results in areas of significant bathymetric relief, and accuracy improves
473 over time by reducing the number of possible locations of the vehicle given the bathymetric history.

474 In this section, we present Algorithm 2, which combines both approaches. By design, we rely on the
475 accuracy of the ocean model predictions over short periods of time at the beginning of plan/mission
476 execution, and augment this with our proposed TBN method which performs well in the areas with poor
477 model predictions and maintains high accuracy over long periods of time. Additionally, we utilize each
478 method to provide estimation bounds for the other to maintain a robust navigation solution. The primary
479 contribution of this proposed combined algorithm is to provide low-power, persistent vehicles with an
480 energy-efficient and accurate navigation solution. The proposed technique can be executed on-board gliders
481 during mission execution, and will significantly aid in keeping them out of high-risk areas, e.g., shipping
482 lanes. Additionally, the TBN portion of the algorithm is able to track deviations from the UKF predicted
483 mission plan, and force surfacings when a threshold error is exceeded. This combined implementation will
484 enable better trajectory tracking by prescribing a surfacing for a GPS fix when necessary; thus maximizing
485 data collection while minimizing time on the surface.

486 Given the method of locomotion for an underwater glider, slow velocities and reduced controllability, the
487 following hybrid algorithm is not intended to provide a means for in situ mission adaptation. The UKF
488 Algorithm functions to provide mission planning and reduce navigational error through the use of ocean
489 model predictions. The TBN Algorithm functions to estimate the position of the glider during mission
490 execution to ensure the vehicle does not drift too far off course. Additionally, the TBN Algorithm provides
491 a method to reconstruct the actual executed path of the vehicle.

492 In the design of Alg. 2, we utilize the predictions from the ocean model to provide an *a priori* plan for
493 mission execution, determining aiming points A_i for each waypoint W_i along with potential surfacing
494 locations within the prescribed mission that meet the desired surfacing interval time or maintain a prescribed
495 error bound as described in Section 3; see Smith et al. (2012b) for further details. In previous work, the UKF
496 Ocean Model Prediction Algorithm maintained an upper bound on navigational error by implementing
497 frequent surfacings to acquire a GPS fix. Here, we are able to relax this constraint by incorporating
498 the LSE/TBN Algorithm to keep navigation error bounded while the vehicle is underway. This enables

Algorithm 2: UKF Ocean Model and TBN Combined Algorithm

Given a mission with n goal waypoints, W_1, \dots, W_n .
 Initiate algorithm upon glider surfacing.
 Acquire current GPS location and updated ROMS (or other) predictions.
 Determine GOAL location.
 Execute UKF Ocean Model Prediction Algorithm to determine a plan for mission execution, i.e., surfacing interval(s) S and aiming point(s) A_i for each waypoint W_i .
 Begin mission execution.
 Total Distance ← Distance between Start Latitude and Longitude (W_i) and Ending Latitude and Longitude (W_{i+1}).
 Execute LSE/TBN Algorithm (Alg. 1).
if error > UKF prescribed 3σ error **then**
 Command a surfacing.
else
 Remain Underwater until next waypoint.
end if
 Determine surfacing error, and adjust computations within the UKF Ocean Model Prediction Algorithm and send updates to the ocean model.

499 longer duration segments underwater, as the glider is free to continue a segment as long as the prescribed
 500 navigational error is not violated. Once a prescribed time epoch has elapsed, or a deviation from the
 501 prescribed path exceeds a set threshold, the glider is commanded to surface. This method enables safer
 502 mission execution coupled with more time for data collection. For each segment of the prescribed path, the
 503 aiming point A_i from the UKF Algorithm is used as the initial compass heading to seed Alg. 1, and this
 504 algorithm is run continuously as data are collected during mission execution.

505 The combined Ocean Model and TBN Algorithm presented in Alg. 2 was implemented on the same 8
 506 SCB missions used for validation of the TBN Algorithm presented in Section 6.1. The UKF Ocean Model
 507 Prediction Algorithm provided 1) the aiming point A_i for each of the mission segments which was used as
 508 the compass heading to seed the TBN Algorithm, and 2) proposed surfacing locations along the path based
 509 on an estimated navigational error. Of the eight total missions, the UKF Algorithm prescribed an additional
 510 surfacing location for only Missions 4 and 7. This surfacing interval was prescribed for 2 hours, based on
 511 the predicted currents from ROMS in the area and the uncertainty computed by the UKF Algorithm. Upon
 512 execution of Alg. 2 the proposed additional surfacing locations for Missions 4 and 7 were not requested or
 513 implemented since the navigational error never exceeded the prescribed 3σ bound of 600 m based on the
 514 TBN Algorithm estimation of location over the duration of the trajectory. However, during Mission 3, the
 515 glider was prescribed to surface less than one hour into the mission since the computed deviation from the
 516 prescribed path based on the TBN Algorithm, exceeded the prescribed 3σ bound of 600 m.

517 As the data used to execute these simulations were the same in situ collected data used to test the TBN
 518 Algorithm in Section 4, the performance results from the TBN portion of Alg. 2 are the same as those listed
 519 in Table 1. We did observe slight differences in the computed path given by Alg. 2 compared to the results
 520 by just applying Alg. 1. These differences were observed during the initial portion of the trajectory, within
 521 the first one to three iterations of executing the TBN portion of Alg. 2. The observed difference is a result
 522 of using the azimuth between the start and goal waypoint for Alg. 1 and the aiming point A_i for Alg. 2 as
 523 the initial compass headings to seed the TBN Algorithm. As pointed out, this did not have an effect on the
 524 overall accuracy of the method, as over the length of the paths, the TBN Algorithm was able to converge to
 525 the same result.

526 Given the experience of multiple implementations of the UKF Ocean Model Prediction Algorithm over
527 many glider missions, it is possible, but unlikely, that the predicted initial compass heading supplied to
528 Alg. 2 may be quite different than the azimuth from prescribed start waypoint to prescribed goal waypoint,
529 e.g., difference $> 90^\circ$. Further experiments are required to analyze the sensitivity of Alg. 2 to the initial
530 compass heading, and are the focus of future work. Additionally, field experiments are planned to validate
531 the promising results shown through these simulated field trials.

8 CONCLUSIONS

532 In this paper, we examined multiple missions that were executed by autonomous gliders in coastal regions
533 in southern California. The results from the field experiments were compared with simulations of the
534 same missions in a UKF that integrated ROMS current predictions and a TBN algorithm for determining
535 location and traversed path underwater. We found that incorporating ocean model predictions does improve
536 navigational accuracy and plan execution, however this method alone neither produces reliable predictions
537 over long periods of time, nor in regions of complex current structure, e.g., shelf break. We found excellent
538 results for localization and path reconstruction in the shallow and shelf-break region using the proposed
539 TBN algorithm. Contrary to the ocean model prediction incorporation, the LSE/TBN Algorithm has an
540 upper bound on error based on the resolution of the underlying bathymetry map, regardless of distance or
541 time traveled. In the majority of areas within the deployment region studied, ROMS provided a prediction
542 of the ocean current that corresponded well with field experiment results. This information can be used to
543 increase the utility of the deterministic model predictions by understanding what regions actually do have
544 *unpredictable* currents.

545 The LSE/TBN Path Estimation algorithm provides a real-time path estimator that provides an improved
546 estimation of the route the glider took over the course of a deployment over existing dead-reckoning
547 solutions. This improved path estimation provides a better understanding of the position of the glider
548 for scientists that utilize the instruments on the glider. It is clear that a combination of the proposed
549 methodologies will provide increased navigational accuracy in this oceanic region for autonomous gliders
550 by forcing a surfacing when a glider veers too far away from the prescribed path.

551 This paper shows the feasibility of a combined approach to mission planning and execution for
552 autonomous gliders to perform persistent monitoring/sampling in coastal ocean regions. Utilizing model
553 predictions for mission planning coupled with a terrain-based navigation while underway has the ability to
554 provide accurate localization estimates for gliders to ~ 100 m, without the use of high-power sensors like
555 DVLs or acoustic communications. This error is approximately $1/5^{th}$ the accuracy previously reported for
556 similar vehicles utilizing dead-reckoning and minimal sensing capabilities Nicholson and Healey (2008);
557 Davis et al. (2009); Smith et al. (2010c, 2012b, 2013). The proposed, combined methodology provides this
558 bound on navigational accuracy regardless of trajectory length or mission duration. The primary application
559 of the proposed method is to bound navigational error for gliders during mission execution, thus keeping
560 them out of high-risk areas like shipping lanes and enabling better trajectory tracking by knowing when a
561 GPS fix is necessary to re-localize.

9 FUTURE WORK

562 In this paper we presented two techniques for operating autonomous gliders for persistent operations. It
563 has been shown that real-time glider navigation accuracy can be increased through the incorporation of
564 ocean model predictions and an Unscented Kalman Filter (UKF) Smith et al. (2010c, 2012a). However,

565 even in this case, the uncertainty grows without bound. In a first step to implement our combined method
566 in a real-time scenario, we utilized it as a means to bound the uncertainty in the UKF. We implemented this
567 algorithm in simulation to demonstrate that we can command a surfacing when the path deviation exceeds
568 a prescribed value. We plan to implement our method online and provide a position estimate for the UKF
569 to compare with at each update epoch. We plan to implement this hybrid system onto a pair of autonomous
570 gliders during field trials in the SCB during summer 2016 to compare with a dead reckoning solution in situ

571 Given the existing research presented earlier on the use of particle filters for TBN for underwater vehicles,
572 we plan to develop a particle filter method for integration within the existing ocean model and UKF
573 framework. This will hopefully provide an online set of navigation tools for accurate localization for
574 underwater vehicles that operate for long duration missions.

575 The study presented here serves as an initial investigation into the comparison of actual ground truth
576 with ocean model predictions. Future work will expand on this effort to include more field trials over
577 longer time periods, as well as to compare other output variables of the model, e.g., salinity, temperature,
578 and chlorophyll, with those measured by the vehicle(s). Additionally, we intend to examine field trials
579 conducted during the same time period over multiple years to examine the ability of the model to predict
580 seasonal and annual variability in the structure of the ocean currents in southern California.

581 Further research includes examining multiple other glider trajectories from USC CINAPS Smith et al.
582 (2010b) to assess algorithm sensitivity, and formalizing and proving the proposed methodology for other
583 AUVs, specifically propeller-driven vehicles such as the YSI EcoMapper AUV Incorporated (2015). The
584 majority of deployments of these vehicles are much shorter than that of the gliders, and will provide a good
585 case study for a lower bound on the applicability of our methods. Also, we will use a YSI EcoMapper
586 vehicle, which includes a 10-beam DVL, to provide accurate ground truth to further benchmark the
587 proposed method. The proposed terrain based navigation method is a complement to other localization
588 systems present for any vehicle. We see this as augmenting existing systems, as well as bounding the
589 inherent errors of other navigation systems, i.e., filtering methods.

590 Note that the presented method is virtually model free, relying only on the vehicle speed for matching
591 measured water depth values with bathymetric maps. In general, the exact vehicle velocity is not known, but
592 approximated and well-bounded. We propose to extend the current method by iterating through reasonable
593 velocities and optimizing over potential trajectory options to determine the best match with gathered data.
594 This will also provide information on the actual speed of the vehicle that can be used in other analyses.

595 As eluded to earlier, many AUV deployments are routine missions carried out in bounded and known
596 locations. We propose to utilize this prior knowledge to improve localization in uncertain environments
597 by updating existing bathymetric maps. Amassing depth data over a deployment region will significantly
598 improve localization for future missions. SCCOOS and the University of Southern California have amassed
599 a large amount of depth data off the coast of Central and Southern California. By combining data of
600 previous missions, better bathymetric maps can be developed and utilized in a TBN framework to augment
601 navigation methods utilized on many vehicles.

DISCLOSURE/CONFLICT-OF-INTEREST STATEMENT

602 The authors declare that the research was conducted in the absence of any commercial or financial
603 relationships that could be construed as a potential conflict of interest.

ACKNOWLEDGMENTS

604 A. Stuntz was supported in part by a Fort Lewis College undergraduate research grant. R.N. Smith was
605 supported in part by a Byron Dare Junior Faculty Award.

REFERENCES

- 606 Alvarez, A., Caiti, A., and Onken, R. (2004). Evolutionary Path Planning for Autonomous Underwater
607 Vehicles in a Variable Ocean. *IEEE Journal of Oceanic Engineering* 29, 418–429
- 608 Anderson, D. M., Glibert, P. M., and Burkholder, J. M. (2002). Harmful Algal Blooms and Eutrophication:
609 Nutrient Sources, Composition, and Consequences. *Estuaries* 25, 704–726
- 610 Anonsen, K. B. and Hallingstad, O. (2006). Terrain aided underwater navigation using point mass and
611 particle filters. In *Proceedings of the IEEE/ION Position Location and Navigation Symposium*
- 612 Anonsen, K. B. and Hallingstad, O. (2007). Sigma point kalman filter for underwater terrain-based
613 navigation. In *Proceedings of the IFAC conference on control applications in marine systems*. 106–110
- 614 Chavez, F. (2010). Canon: Controlled, Agile, and Novel Observing Network - <http://www.mbari.org/canon>
- 615 Davis, R. E., Leonard, N. E., and Fratantoni, D. M. (2009). Routing strategies for underwater gliders. *Deep*
616 *Sea Research Part II: Topical Studies in Oceanography* 56, 173–187. doi:10.1016/j.dsr2.2008.08.005
- 617 Davis, R. E., Ohman, M. D., Rudnick, D. L., Sherman, J. T., and Hodges, B. (2008). Glider surveillance of
618 physics and biology in the southern California Current System. *Limnol. Oceanogr.* 53, 2151–2168
- 619 Ferrari, R. (2011). Ocean science. A frontal challenge for climate models. *Science (New York, N.Y.)* 332,
620 316–7. doi:10.1126/science.1203632
- 621 Flenniken, W., Wall, J., and Bevely, D. (2005). Characterization of various imu error sources and the effect
622 on navigation performance. In *ION GNSS*. 967–978
- 623 Fulton-Bennett, K. (2005). Canyons, currents, and algal blooms - How Monterey Canyon influences the
624 growth of microscopic marine algae
- 625 Garau, B., Alvarez, A., and Oliver, G. (2005). Path Planning of Autonomous Underwater Vehicles in
626 Current Fields with Complex Spatial Variability: an $\{A\}^*$ Approach. In *Proceedings of the IEEE*
627 *International Conference on Robotics and Automation* (Barcelona, Spain)
- 628 Godin, M. A., Bellingham, J. G., Rajan, K., Chao, Y., and Leonard, N. E. (2006). A collaborative portal for
629 ocean observatory control. In *Proceedings of the Marine Technology Society / Institute of Electrical and*
630 *Electronics Engineers Oceans Conference* (Boston, MA)
- 631 Golden, J. P. (1980). Terrain contour matching (tercom): a cruise missile guidance aid. In *24th Annual*
632 *Technical Symposium* (International Society for Optics and Photonics), 10–18
- 633 Griffiths, G., Jones, C., Ferguson, J., and Bose, N. (2007). Undersea gliders. *Journal of Ocean Technology*
634 2, 64–75
- 635 Gustafsson, F., Gunnarsson, F., Bergman, N., Forssell, U., Jansson, J., Karlsson, R., et al. (2002). Particle
636 filters for positioning, navigation, and tracking. *Signal Processing, IEEE Transactions on* 50, 425–437
- 637 Hollinger, G. A., Englot, B., Hover, F., Mitra, U., and Sukhatme, G. S. (2012). Uncertainty-Driven View
638 Planning for Underwater Inspection. In *IEEE International Conference on Robotics and Automation* (St.
639 Paul, MN), 4884–4891
- 640 Horner, R. A., Garrison, D. L., and Gerald, F. (1997). Harmful algal blooms and red tide problems on the
641 U.S. west coast. *Limnology and Oceanography* 42, 1076–1088
- 642 Huster, A. and Rock, S. M. (2003). Relative Position Sensing by Fusing Monocular Vision and Inertial
643 Rate Sensors. In *Proceedings of the 11th International Conference on Advanced Robotics* $\{(ICAR'03)\}$
644 (Coimbra, Portugal), vol. 3, 1562–1567

- 645 Incorporated, Y. (2015). YSI EcoMapper - <http://www.ysi.com/productsdetail.php?EcoMapper-41>
- 646 Jones, B. H., Noble, M. A., and Dickey, T. D. (2002). Hydrographic and particle distributions over the
647 Palos Verdes Continental Shelf: spatial, seasonal and daily variability. *Continental Shelf Research* 22,
648 945–965
- 649 Julier, S. J. and Uhlmann, J. K. (2004). Unscented filtering and nonlinear estimation. *Proceedings of the*
650 *IEEE* 92, 401–422
- 651 Kinsey, J. C., Eustice, R. M., and Whitcomb, L. L. (2006). A survey of underwater vehicle navigation:
652 Recent advances and new challenges. In *IFAC Conference of Manoeuvring and Control of Marine*
653 *Craft*
- 654 Kruger, D., Stolkin, R., Blum, A., and Briganti, J. (2007). Optimal AUV path planning for extended
655 missions in complex, fast-flowing estuarine environments. In *Proceedings of the IEEE International*
656 *Conference on Robotics and Automation* (Rome, Italy)
- 657 Kudela, R., Pitcher, G., Probyn, T., Figueiras, F., Moita, T., and Trainer, V. (2005). Harmful Algal Blooms
658 in coastal upwelling systems. *Oceanography* 18(2), 184–197
- 659 Lagadec, J. (2010). *Terrain Based Navigation using a Particle Filter for Long range glider missions -*
660 *Feasibility study and simulations*. Master's thesis, ENSIETA Ecole Nationale Supérieure DIngenieurs
- 661 Mancho, A. M., Hernández-García, E., Small, D., Wiggins, S., and Fernández, V. (2008). Lagrangian
662 Transport through an Ocean Front in the Northwestern Mediterranean Sea. *Journal of Physical*
663 *Oceanography* 38, 1222–1237. doi:10.1175/2007JPO3677.1
- 664 Nicholson, J. W. and Healey, A. J. (2008). The Present State of Autonomous Underwater Vehicle
665 (AUV) Applications and Technologies. *Marine Technology Society Journal* 42, 44–51. doi:doi:
666 10.4031/002533208786861272
- 667 Ono, M. and Williams, B. C. (2008). An Efficient Motion Planning Algorithm for Stochastic Dynamic
668 Systems with Constraints on Probability of Failure. In *Proceedings of the Twenty-Third AAAI Conference*
669 *on Artificial Intelligence*
- 670 Paley, D., Zhang, F., and Leonard, N. (2008). Cooperative control for ocean sampling: The glider
671 coordinated control system. *IEEE Transactions on Control Systems Technology* 16, 735–744. doi:10.
672 1109/TCST.2007.912238
- 673 Pereira, A. A., Binney, J., Hollinger, G. A., and Sukhatme, G. S. (2013). Risk-aware Path Planning
674 for Autonomous Underwater Vehicles using Predictive Ocean Models. *Journal of Field Robotics* 30,
675 741–762. doi:10.1002/rob.21472
- 676 Powell, B. S., Arango, H. G., Moore, A. M., Lorenzo, E. D., Milliff, R. F., and Foley, D. (2008). 4DVAR
677 data assimilation in the Intra-Americas Sea with the Regional Ocean Modeling System (ROMS). *Ocean*
678 *Modelling* 25, 173–188. doi:10.1016/j.ocemod.2008.08.002
- 679 Rao, D. and Williams, S. B. (2009). Large-scale path planning for Underwater Gliders in ocean currents.
680 In *Proceedings of the Australasian Conference on Robotics and Automation* (Sydney)
- 681 Rixen, M., Book, J. W., Carta, A., Grandi, V., Gualdesi, L., Stoner, R., et al. (2009). Improved ocean
682 prediction skill and reduced uncertainty in the coastal region from multi-model super-ensembles. *Journal*
683 *of Marine Systems* 78, Supple, S282 – S289. doi:10.1016/j.jmarsys.2009.01.014
- 684 SCCOOS (2009). SCCOOS: Southern California Coastal Observing System - <http://www.sccoos.org>
- 685 Schnetzer, A., Miller, P. E., Schaffner, R. A., Stauffer, B., Jones, B. H., Weisberg, S. B., et al. (2007).
686 Blooms of Pseudo-nitzschia and Domoic Acid in the San Pedro Channel and Los Angeles harbor areas
687 of the Southern California Bight, 2003-2004. *Harmful Algae* 6, 372–387
- 688 Schofield, O., Kohut, J., Aragon, D., Creed, E., Graver, J., Haldman, C., et al. (2007). Slocum gliders:
689 Robust and ready. *Journal of Field Robotics* 24, 473–485

- 690 Sekula-Wood, E., Schnetzer, A., Benitez-Nelson, C. R., Anderson, C., Berelson, W., Brzezinski, M., et al.
691 (2009). The Toxin Express: Rapid downward transport of the neurotoxin domoic acid in coastal waters.
692 *Nature Geosciences* 2, 273–275. doi:10.1038/ngeo472
- 693 Smith, R. N., Chao, Y., Li, P. P., Caron, D. A., Jones, B. H., and Sukhatme, G. S. (2010a). Planning and
694 implementing trajectories for autonomous underwater vehicles to track evolving ocean processes based
695 on predictions from a regional ocean model. *International Journal of Robotics Research* 29, 1475–1497.
696 doi:10.1177/0278364910377243
- 697 Smith, R. N., Das, J., Heidarsson, H., Pereira, A., Cetinić, I., Darjany, L., et al. (2010b). {USC} {CINAPS}
698 Builds Bridges: Observing and Monitoring the {S}outhern {C}alifornia {B}ight. *IEEE Robotics and
699 Automation Magazine, Special Issue on Marine Robotics Systems* 17, 20–30
- 700 Smith, R. N., Kelly, J., Chao, Y., Jones, B. H., and Sukhatme, G. S. (2010c). Towards Improvement of
701 Autonomous Glider Navigation Accuracy through the use of Regional Ocean Models. In *Proceedings of
702 the 29th International Conference on Offshore Mechanics and Arctic Engineering* (Shanghai, China),
703 597–606
- 704 Smith, R. N., Kelly, J., Nazarzadeh, K., and Sukhatme, G. S. (2013). An Investigation on the Accuracy of
705 Regional Ocean Models Through Field Trials. In *Proceedings of the IEEE International Conference on
706 Robotics and Automation*
- 707 Smith, R. N., Kelly, J., and Sukhatme, G. S. (2012a). Towards improving mission execution for autonomous
708 gliders with an ocean model and kalman filter. *2012 IEEE International Conference on Robotics and
709 Automation* , 4870–4877doi:10.1109/ICRA.2012.6224609
- 710 Smith, R. N., Kelly, J., and Sukhatme, G. S. (2012b). Towards improving mission execution for autonomous
711 gliders with an ocean model and Kalman filter. In *Proceedings - IEEE International Conference on
712 Robotics and Automation*. 4870–4877
- 713 Smith, R. N., Schwager, M., Smith, S. L., Jones, B. H., Rus, D., and Sukhatme, G. S. (2011a). Persistent
714 ocean monitoring with underwater gliders: Adapting sampling resolution. *Journal of Field Robotics* 28,
715 714 – 741
- 716 Smith, R. N., Schwager, M., Smith, S. L., Rus, D., and Sukhatme, G. S. (2011b). Persistent ocean
717 monitoring with underwater gliders: Towards accurate reconstruction of dynamic ocean processes. In
718 *Proceedings - IEEE International Conference on Robotics and Automation*. 1517–1524
- 719 Stevens, B. L. and Lewis, F. L. (2003). *Aircraft Control and Simulation* (Wiley-Interscience), Second edn.
- 720 Stuntz, A., Liebel, D., and Smith, R. N. (2015). Increasing Navigation Accuracy and Localization for
721 Autonomous Gliders to Enable Persistent Autonomy. In *MTS/IEEE Oceans* (Genova, Italy)
- 722 Taylor, J. R. (1996). An introduction to error analysis: The study of uncertainties in physical measurements
723 , 166–168
- 724 Vu, Q. (2008). JPL: OurOcean Portal - <http://ourocean.jpl.nasa.gov>
- 725 Webb Research Corporation (2008). Slocum glider. [http://www.webbresearch.com/slocum.](http://www.webbresearch.com/slocum.htm)
726 [htm](http://www.webbresearch.com/slocum.htm). Viewed March 2011
- 727 Whitcomb, L., Yoerger, D., Singh, H., and Howland, J. (1999). Advances in underwater robot vehicles
728 for deep ocean exploration: Navigation, control, and survey operations. In *Proceedings of the Ninth
729 International Symposium of Robotics Research* (Snowbird, UT: Springer-Verlag), 439–448
- 730 Witt, J. and Dunbabin, M. (2008). Go with the flow: Optimal path planning in coastal environments. In
731 *Proceedings of the 2008 Australasian Conference on Robotics & Automation (ACRA 2008)*, eds. J. Kim
732 and R. Mahony (Canberra, ACT). ISBN: 9780646506432

- 733 Zhang, Y., Bellingham, J. G., Ryan, J. P., Kieft, B., and Stanway, M. J. (2013). Two-dimensional mapping
734 and tracking of a coastal upwelling front by an autonomous underwater vehicle. In *MTS/IEEE Oceans -*
735 *San Diego*. 1–4

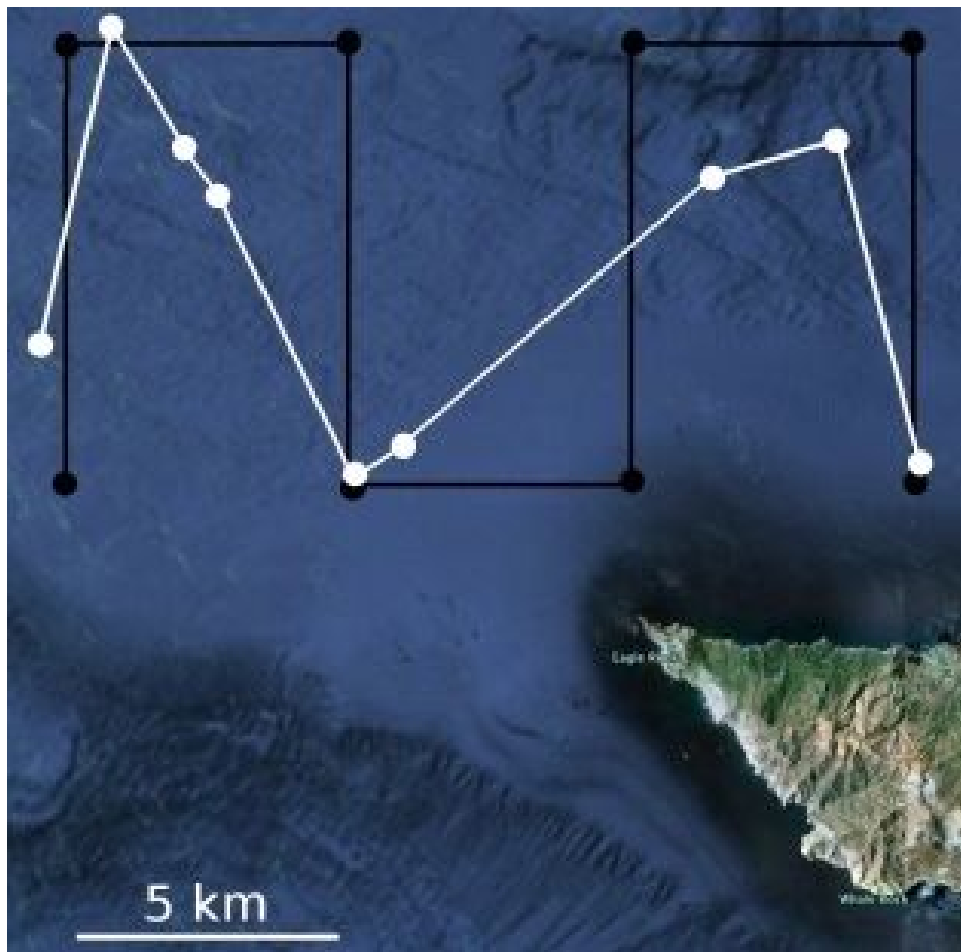


Figure 1. Planned lawnmower pattern (black waypoints and path) and the actual executed path (white surfacing locations and path) for a glider deployment off of the northern tip of Santa Catalina Island, CA.

FIGURES



Figure 2. A CINAPS Smith et al. (2010b) Slocum glider preparing to start a mission off the Northeast coast of Santa Catalina Island, CA.

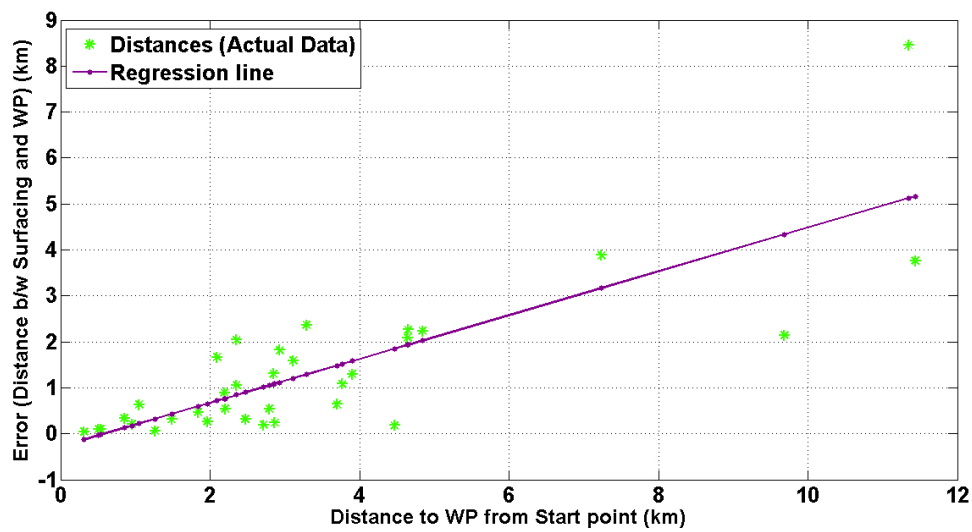


Figure 3. A plot of the absolute surfacing error (in km) versus the length of the prescribed trajectory for the actual field trials.

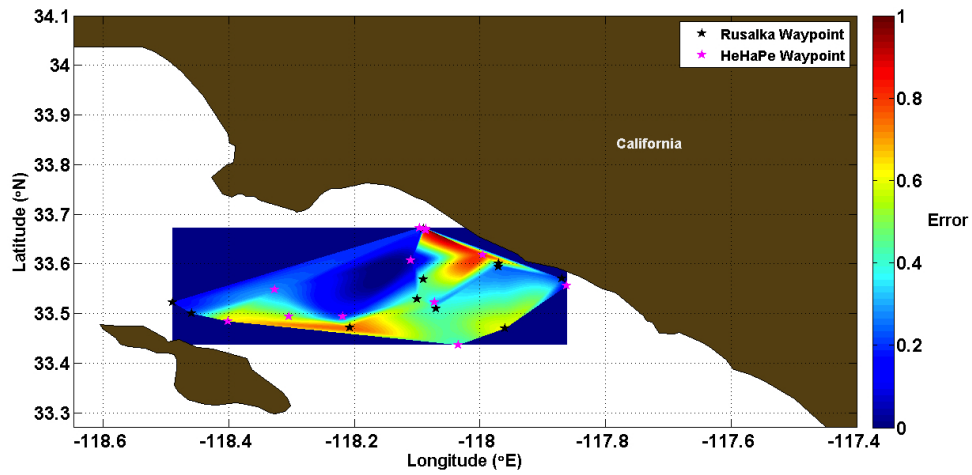


Figure 4. A heat-map surface plot representing the normalised error between the surfacing location and the prescribed waypoint for the actual field trials.

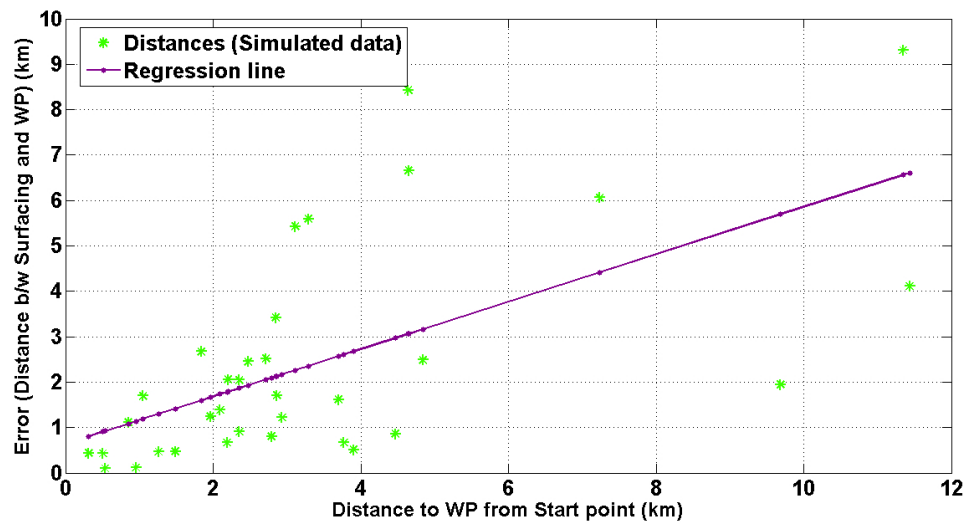


Figure 5. A plot of the absolute surfacing error (in km) versus the length of the prescribed trajectory for the simulated trials.

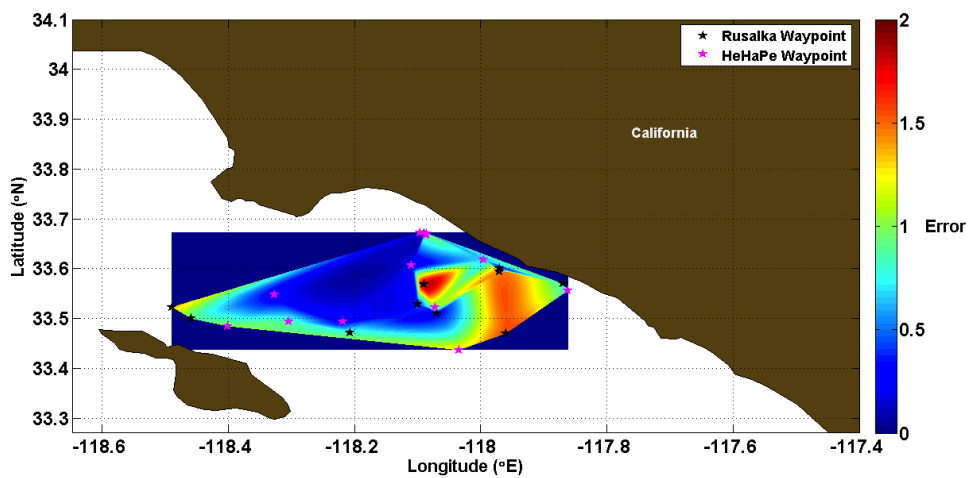


Figure 6. A heat-map surface plot representing the normalised error between the surfacing location and the prescribed waypoint for the simulated trials.

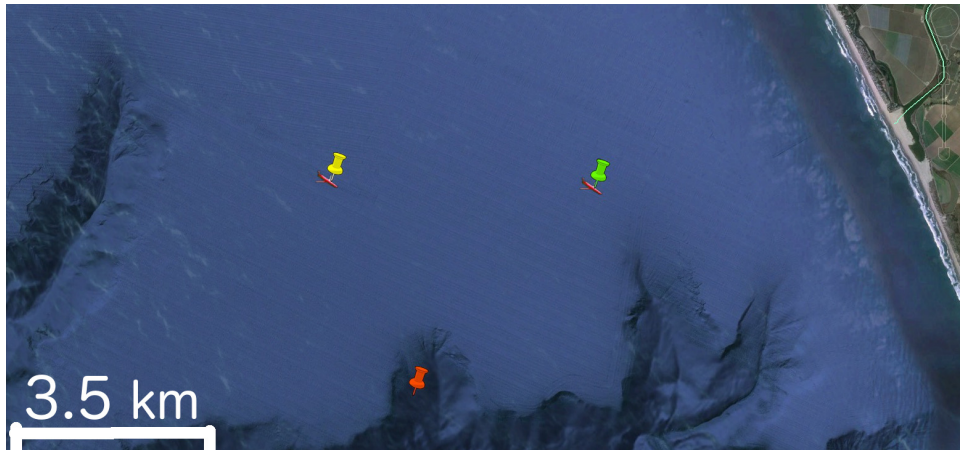


Figure 7. The start position and end position are the yellow and green pins on the map, respectively. The goal position of the glider is the red pin on the map. The straight line (inaccurate) path of the glider is assumed to connect the yellow pin and the green pin. Image courtesy of Google Earth.

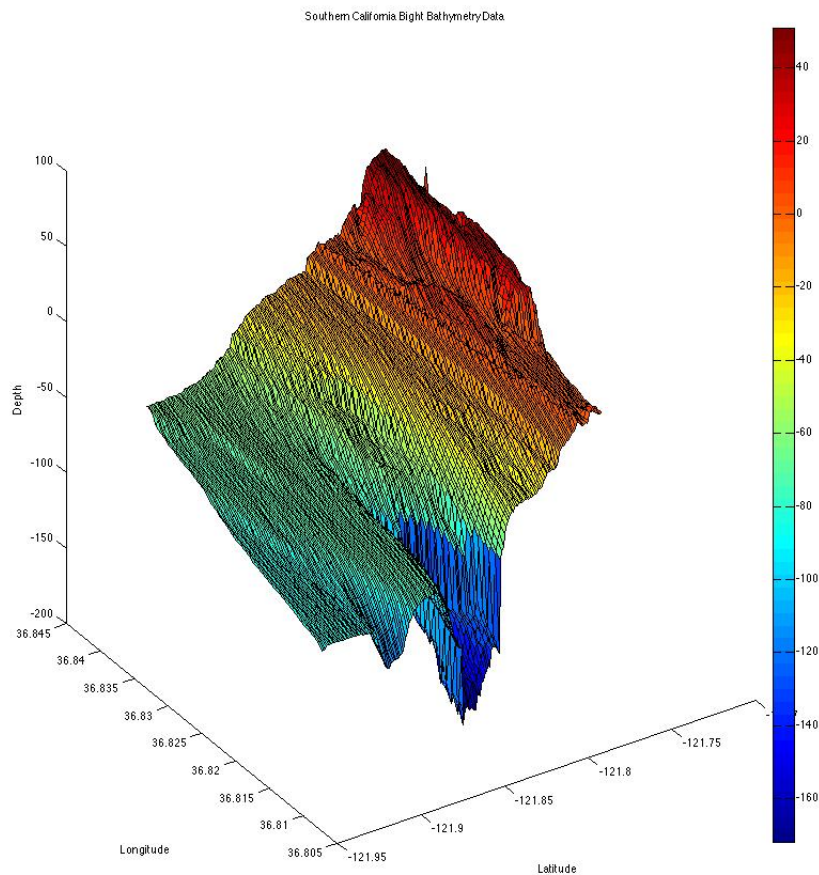


Figure 8. Bathymetry data mapped and shaded, showing detail of the SCCOOS data in Monterey Bay. Maps are accurate to 0.0008° in both latitude and longitude.

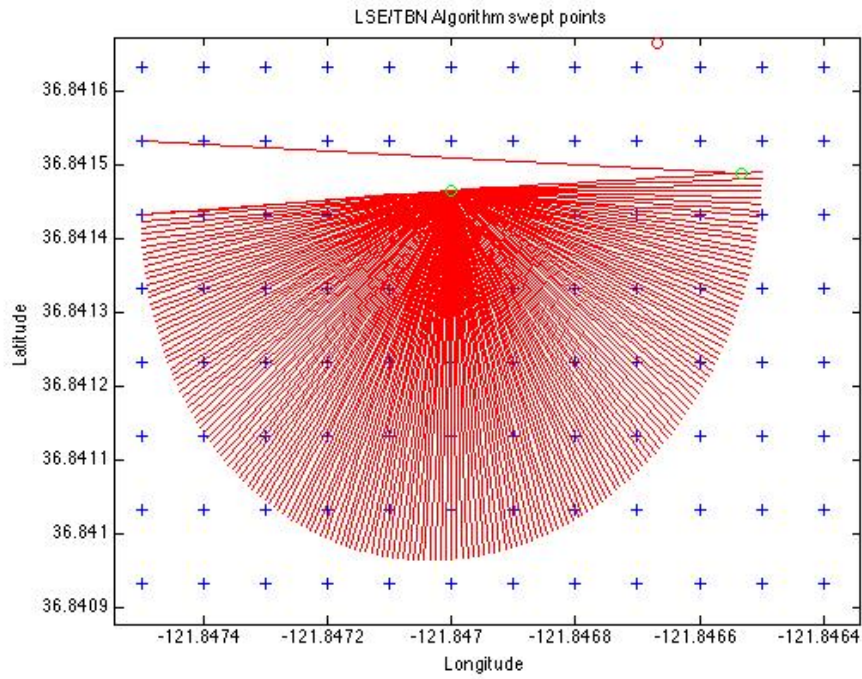


Figure 9. Path options generated around the start Latitude and Longitude. 180 path options are shown in red.

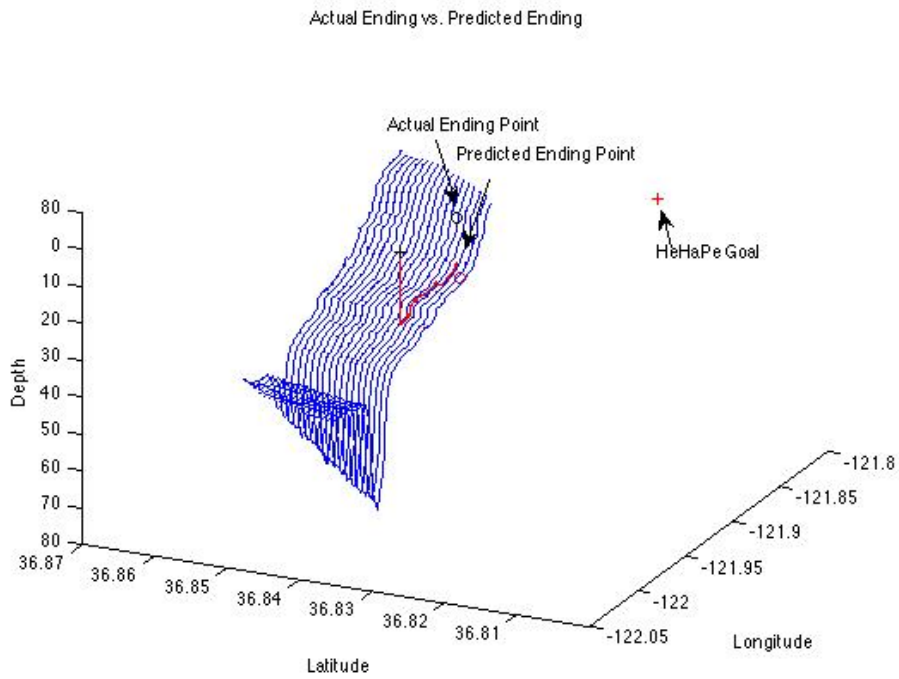


Figure 10. Final results comparing the predicted ending point and the actual ending point. The prescribed goal location is also plotted, demonstrating the more than 4000m dead-reckoning error.

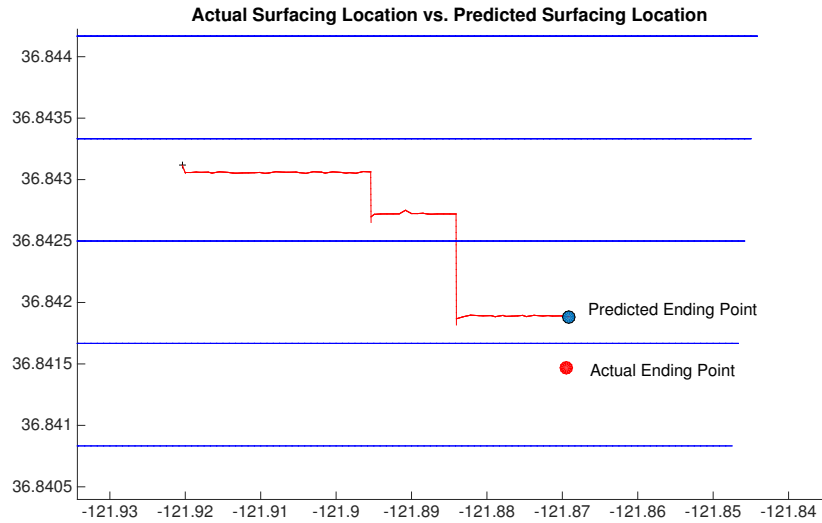


Figure 11. The path on top of the bathymetry data. Showing the progression of the path as it nears the its final predicted point.

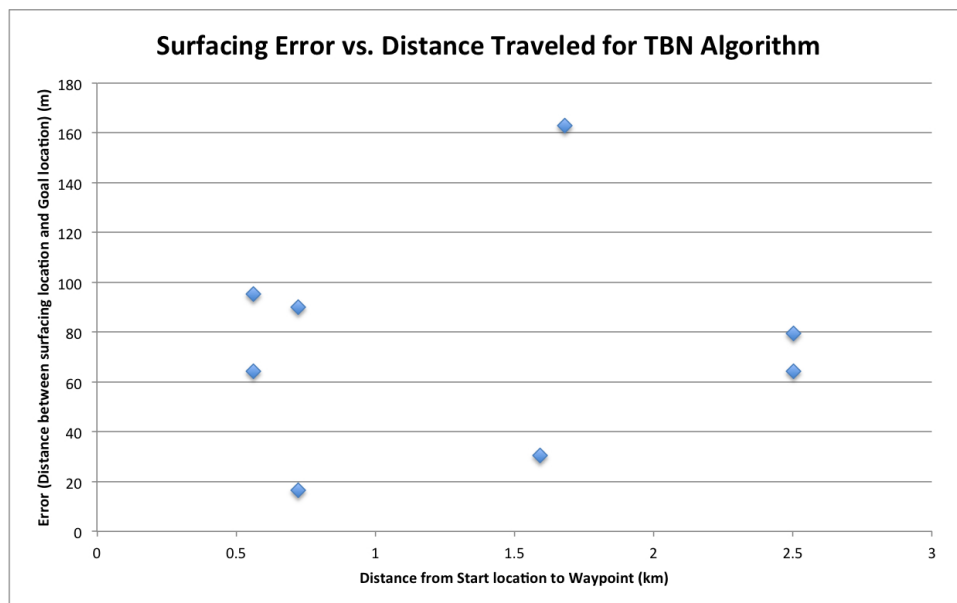


Figure 12. A plot of the TBN predicted surfacing error in meters versus the length of the prescribed trajectory in kilometers.

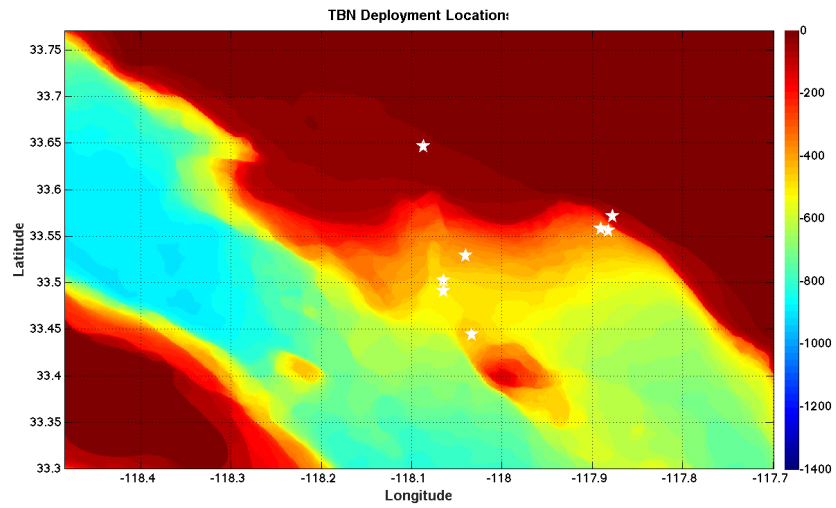


Figure 13. The locations of the eight missions examined with the TBN algorithm overlaid on a bathymetric heat map of the SCB.

736 Table 1: Results of applying the TBN Algorithm to multiple missions in the Southern California Bight.
 737 All distances are presented in meters.

	TBN Path Length	Prescribed Path Length	TBN to Actual Surface Location	TBN to Actual Goal	Actual Surface to Actual Goal
Mission 1	737	722.88	16.4208	14.6689	23.9244
Mission 2	603	563.267	64.3373	187.9952	128.6411
Mission 3	1622	1592.8	30.3678	1562.5	1585.1
Mission 4	2566.2	2502.9	64.1873	132.4565	191.4795
Mission 5	1072.8	722.9	90.03	826.7	23.92
Mission 6	624	563.3	95.23	716.9	128.64
Mission 7	2520.3	2502.9	79.56	204.4	191.48
Mission 8	1717.6	1681.9	162.9	314.9	268.0